STUDY OF AERODYNAMIC NOISE GENERATED FROM A FORWARD CURVED FAN DUE TO ROTATING STALL CELL

Soichi SASAKI[1], Yuta ONOMICHI[2]

[1] *Division of System Science, Nagasaki University, Nagasaki 852-8521, Japan*

[2] *Department of Advanced Enginering, Nagasaki University, Nagasaki, 852-8521, Japan*

SUMMARY

In order to clarify the influence of rotating stall cell on the properties of a forward curved fan, we experimentally estimated the aerodynamic characteristics and noise of the two different fans. At the front shroud of the forward curved fan without shroud (MF9), the rotating stall cells formed due to the blade tip leakage vortex. The cells formed the pseudo blades in the circumferential direction of the impeller. The fan having impeller with shroud (MF9S) hardly formed the rotating stall cells. From these results, the broadband noise level of MF9S in the low frequency domain became large than that of the MF9 at the vicinity of the rotating frequency of the rotating stall cell.

INTRODUCTION

The contained in architectural materials such as formaldehyde (formalin) caused serious problem on the human body since a lot of house is constructed with the tightly airtight. This is an issue which is called as “Sick House Syndrome”. Depending on this problem, Japanese Government revised the building code in 2003 [1]. The setup of the equipment that can be ventilated through 24 hours was obligated to the house newly constructed. For such a ventilation system, a forward curved fan is often applied. Thus, it became necessary not only to increase fan efficiency but also to decrease fan noise in order to ensure a comfortable living environment. When such a ventilation system is developed, reduction of the fan noise becomes major technical issue.

The fan noise is roughly categorized to the broadband noise and the discrete frequency noise which is interaction between the wake of the impeller and the tongue in the diffuser. Datong et al. clarified that the optimization of the shape of the tongue of a forward curved fan can not only control the fan

noise but also expand the effective operation point [2]. Suárez et al. pointed out that the optimization of the geometry of the tongue is effective for decreasing the fan noise [3-5]. Ohta et al. [6] implied that the intensity of the noise source was estimated by the quasi-steady model; in the model, the wake of the blade impinges to the tongue. In order to predict the acoustic pressure in the far field, Younsi et al. [7] applied the unsteady flow variables provided by the CFD calculations as inputs in the Ffowcs Williams-Hawkings equations [8]. As results of the prediction, the discrete frequency noise agreed well with the measured noise level. These previous studies were analysis for the discrete frequency noise in the blade passing frequency.

On the other hand, Longhouse presented the effect of the optimization of the shroud for the noise reduction [9]. However, the experimental study of the broadband noise of the forward curved fan, in particular, there is little study on the influence of the front shroud on the improvement of the fan performance. Therefore, in this study, we experimentally estimate the influence of the shroud on the aerodynamic characteristics and noise of a forward curved fan. Based on the actual measured characteristics and the numerical simulation of the internal flow, the influence of the rotating stall cell on the broadband noise is discussed.

EXPERIMENTAL SETUP

The test impeller is shown in Figure 1 and its main dimensions are summarized in Table 1. These impellers are the forward curved centrifugal type. The two dimensional forward curved blade is employed for the impeller of the fan. The diameter of the impellers is 125 mm, the number of blades is 40; the span length is 50 mm. In the following explanation, the fans with shroud and without shroud are referred to as MF9 and MF9S, respectively.

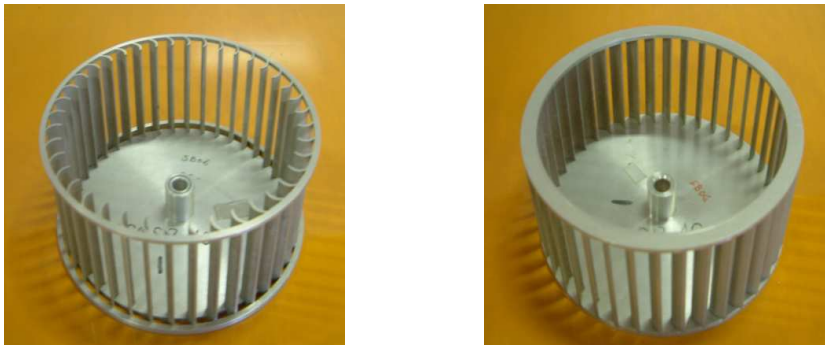

(a) MF9 *(b) MF9S*

Figure 1: Test impeller

Table 1: Main dimensions of the test impeller

Impeller	MF9	MF9S
Diameter , D (mm)	125	
Chord Length , C (mm)	9	
Number of Blades , Z	40	
Span Length , b (mm)	50	
Shroud	without shroud	with shroud

The experimental apparatus used for measuring the aerodynamic characteristics of the fan is shown in Figure 2. The static pressure was measured in the plenum chamber, which has dimensions of 500

mm × 500 mm× 900 mm. The normalized aerodynamic characteristics of the fan are defined as Equation (1).

$$\psi = \frac{2P_s}{\rho U^2}, \phi = \frac{Q}{60\,\pi\, D\, b\, U}$$
$$\lambda = \frac{2L}{\rho\,\pi\, D\, b\, U^3}, \eta = \frac{\varphi\,\psi}{\lambda} \quad (1)$$

where ψ is the static pressure coefficient, φ is the flow coefficient, λ is the power coefficient, and η is the efficiency. The rotational speed was set to 2800 rpm. The noise was measured using a noise level meter (ONO SOKKI, LA4350) at an observation point that was 1.0 m above the bell mouth and situated along the axis of the motor. The noise data were input to FFT analyzer (ONO SOKKI, CF5210) to evaluate the noise spectrum. When the fan noise is measured in this experiment, the subsidiary fan is detached from this experimental setup. At this time, the flow rate of the fan is adjusted based on the static pressure characteristics in the fan exit measured beforehand.

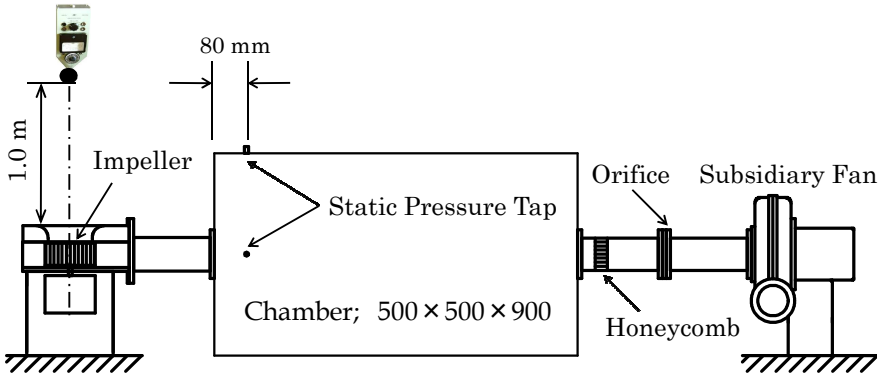

Figure 2: Experimental apparatus

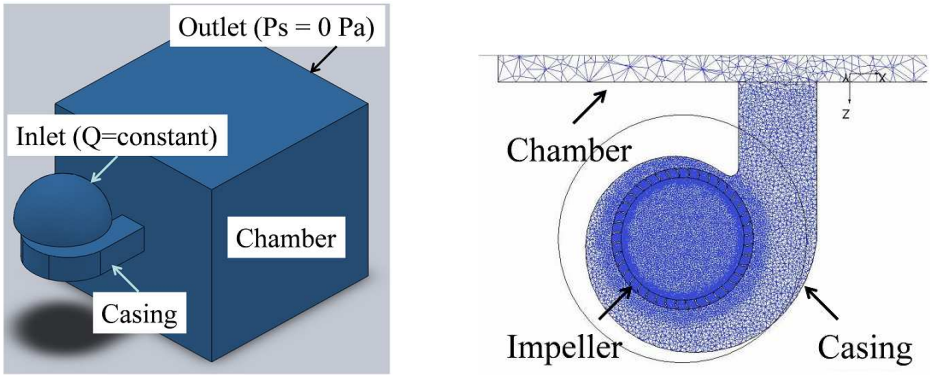

(a) CAD model *(b) 2 dimensional mesh of the fan*

Figure 3: Model for the numerical simulation

The three-dimensional model of the fan for the CFD is shown in Figure 3. Figure 3 (a) is the CAD model and Figure 3 (b) is the two-dimensional calculation mesh. The representative length of the impeller and the diffuser is modeled equivalently to the actual system. The 500 mm ×500 mm × 500 mm chamber was attached to the outlet of the diffuser. The CFD code of SCRYU/Tetra produced by Software Cradle Co., Ltd. was used for the numerical simulations. Approximately 4.5 million grid elements were employed to solve the entire unsteady flow field of the fan. A constant flow rate was set at the inlet boundary of the model; the atmospheric pressure (0 Pa) was given to the outlet side. For the initial condition of the numerical simulation, the steady turbulent flow field was

calculated by standard k-ε model in advance. Then, the unsteady flow field is calculated by the LES; the turbulent flow field is developed in the iteration as five times rotation of the impeller.

RESULTS AND DISCUSSION

The aerodynamic characteristics of the fan are compared in Figure 4. The pressure of MF9S which is the fan with the shroud becomes higher than MF9 over the wide flow rate domain. The pressure rise of MF9S improves the efficiency at the maximum efficiency point (φ = 0.15) 1.6% than the pressure of MF9. The pressure coefficient analyzed by the numerical simulation at φ = 0.1 and φ = 0.15 agreed well with the measured pressure level.

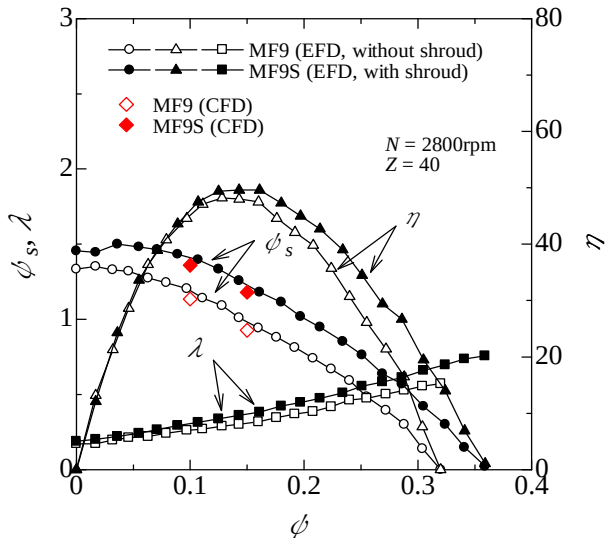

Figure 4: Aerodynamic characteristics

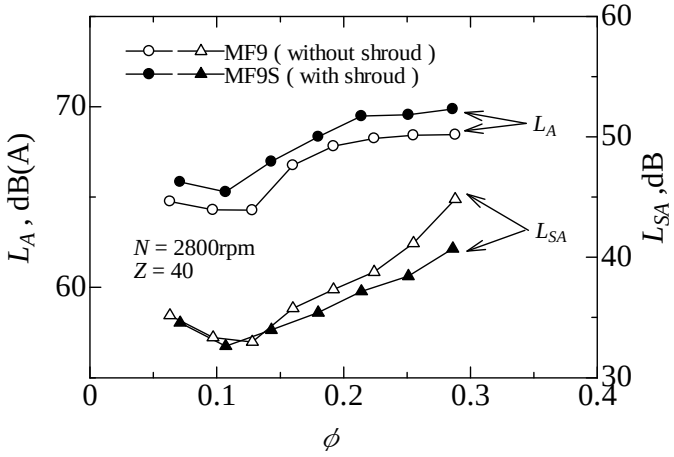

Figure 5: Noise characteristics

In Figure 5, the noise characteristics of two fans are compared. The circular dots are the noise level; the triangle dots are the specific noise level. Specific noise is a characteristic that is related to the aerodynamic characteristics of the fan and its noise level. The specific noise level means the noise level per the unit flow rate and per the unit total pressure. When the level of the specific noise level becomes small, the fan is regarded to as comprehensively excellent. The noise characteristics indicate that the MF9S becomes larger than that of the MF9 without shroud. The both

characteristics increase the noise level approximately from φ = 0.1 to 0.2. We do not discuss the characteristics within present study because the characteristics may be caused by the BPF noise. The specific noise level of MF9S becomes small than MF9 in the domain of the high flow rate than that of the maximum efficiency point. These results indicate the comprehensive characteristics of the MF9S are improved in the high flow rate domain.

In Figure 6, the two noise spectra at flow rate coefficient φ = 0.1 are compared. The overall noise level of MF9S becomes 1 dB(A) large than that of MF9. The difference of the noise level occurred in the vicinity of 200 Hz of the spectra.

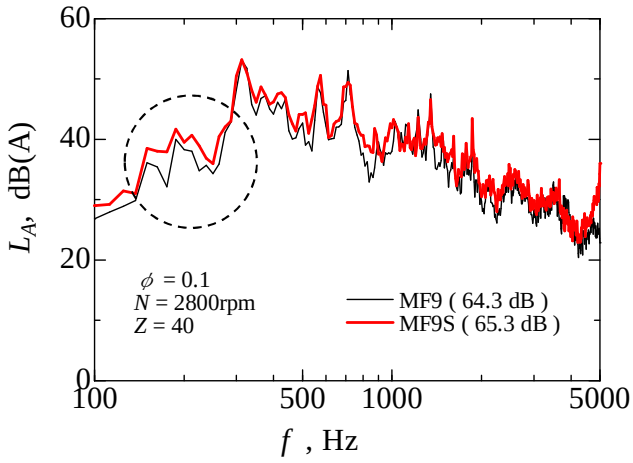

Figure 6: Spectrum distribution of the fan noise

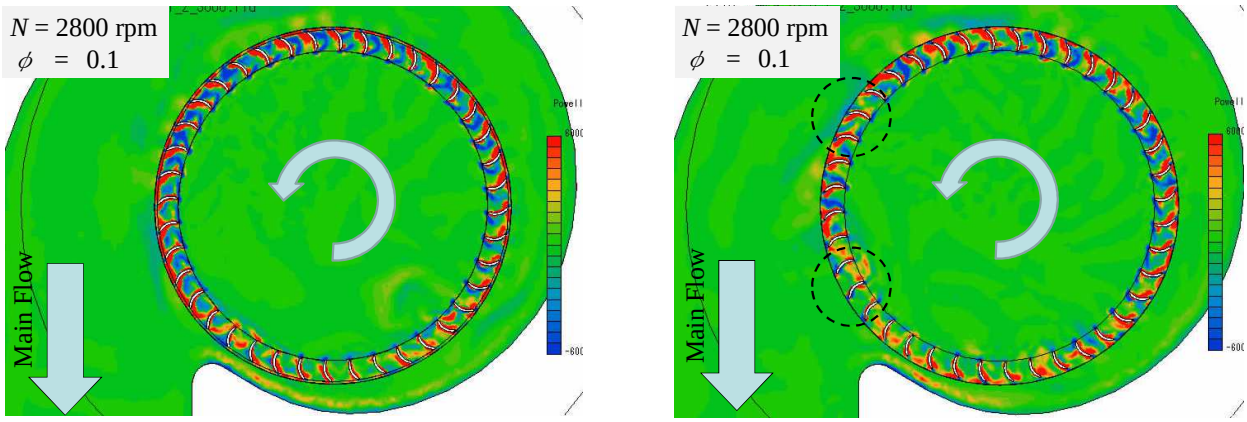

(a) MF9S *(b) MF9*

Figure 7: Visualization on the aerodynamic sound source (z = 35 mm)

The distributions in the two-dimensional section of the source term of "Powell–Howe" visualized by the numerical simulation are shown in Figure 7. The location of the analyzed section is 35 mm from the rear shroud. Powell [10] studied the theoretical sound sources in a flow field, and Howe [11] mathematically expressed the sound source as Equation (2).

$$\frac{\partial^2 p_a}{\partial t^2} - c^2 \nabla^2 p_a = \rho_0 div(\vec{\omega} \times \vec{u}) \tag{2}$$

where $\vec{\omega}$ is the vorticity vector and $\vec{u}$ is the velocity vector. The spatial distribution of the sound source can be visualized by using the right-hand side of Equation (2). In the both impellers, the

strong noise sources are generated in the blade passage. In the case of MF9, the distribution of the periodical aerodynamic noise source is not formed in the wake, whereas, in the case of MF9, the positive and negative noise source which is larger than that of blade pitch is alternately generated in the wake.

In Figure 8, the velocity vector of the absolute velocity around the impeller is shown. The position of the section is same as Figure 7 (z = 35 mm). In the velocity distribution of MF9S, the distribution of the uniform velocity which flows to the outward is formed. In the case of MF9, the velocity becomes low speed at the location where the noise source became neutral. Thus, the velocity distribution does not become uniform. In this simulation, the time step for the calculation is defined that the one pitch is divided into ten steps. Thus, when the simulation iterates 100 steps, the blade is moved into 10 pitches to circumferential direction. However, the center of the stalled domain of the velocity moved only four pitches of the blades after the 100 steps. Therefore, these results indicate that rotational speed of stalled domain may be 40 % of rotation of the impeller. Here, the stalled domain in MF9 is named to as the rotating stall cell. The rotating frequency of the rotating stall cell is defined as Equation (3).

$$f = N_c \, Z_c / 60 \tag{3}$$

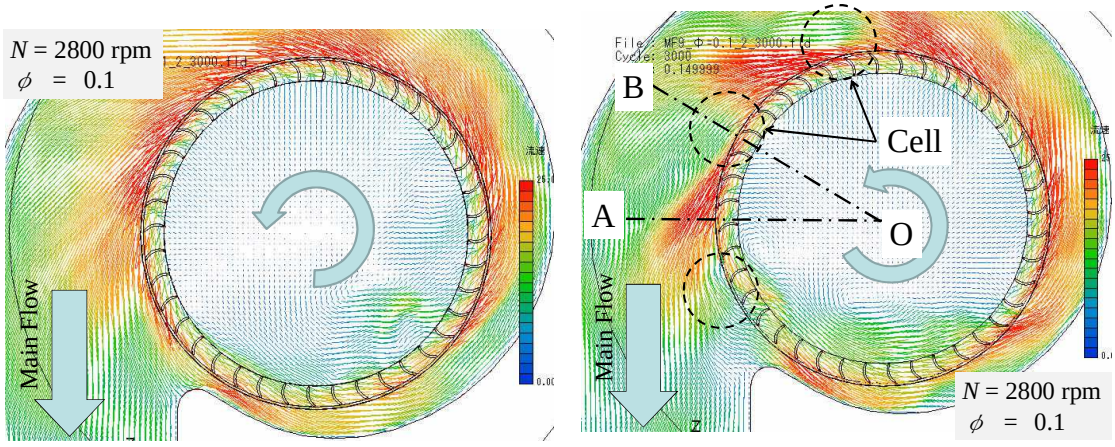

(a) MF9S *(b) MF9*

Figure 8: Velocity distribution in the 2-dimentional section (z = 35 mm)

where, the N_c is the rotation speed of rotating stall cell, the Z_c is the number of rotating stall cell. Since one developed rotating stall cell is formed in the six blades, the approximately seven cells may be formed around the impeller. In this case, the rotating frequency of the cell becomes 130 Hz. The rotating frequency exists in the vicinity of frequency band of the measured broadband noise confirmed in Figure 6. In the case of MF9, the non-uniform noise sources formed at the front shroud side. These results imply that the broadband noise level of MF9 in the low frequency synchronized with the rotating frequency of the rotating stall cell becomes relatively small than that of the MF9S.

The velocity vector in the meridian plane is shown in Figure 9. Figure 9 (a) is the flow regime in the section without the rotating stall cell (O-A section in Figure 8); Figure 9 (b) is the flow regime in the section with the rotating stall cell (O-B section in Figure 8). The main flow domain radiated toward the outside is formed at the rear shroud side; the effective flow of a fan flows out from this domain. In the flow regime of Fig. 9 (a), the vortical recirculation flow is formed at the front shroud side. On the other hand, in the case Figure (b), the recirculation domain is expanded; the main flow domain becomes narrow. The static pressure of the fan increases at the main flow domain. These results imply that the static pressure of MF9 with rotating stall cell induces the pressure drop due to the decrease of the main flow domain.

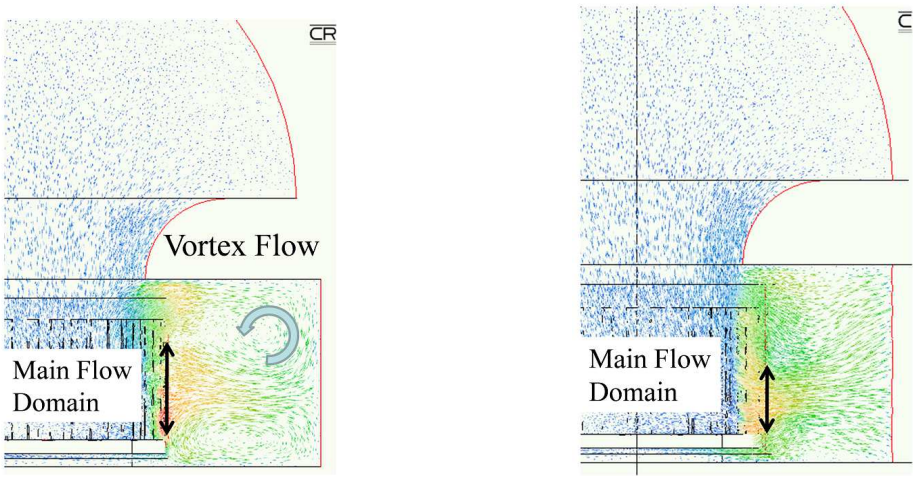

(a) without the cell (O - A section) *(b) with the cell (O - B section)*

Figure 9: Velocity distribution in the meridian section

In Figure 10, the pressure distribution around the impeller of MF9 is shown. In the vicinity of the front shroud side of the impeller, the vortical low pressure domain is formed. This low pressure domain indicates the center of the tip leakage vortex from the pressure surface side to the suction surface side. The outward flow is obstructed by the blade tip leakage flow; as results, the rotating stall cell is formed. Moreover, the aerodynamic noise source due to the rotating stall becomes weak because the flow stagnates at the same position; from these reasons, the noise level of MF9 becomes small than that of MF9S.

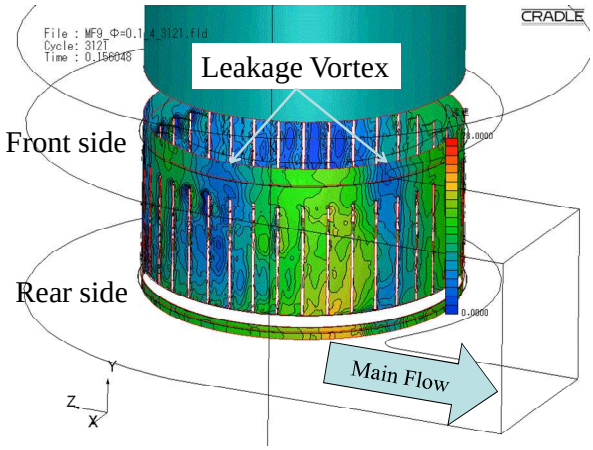

Figure 10: Pressure distribution around the impeller without the shroud (MF9)

CONCLUSIONS

1. At the front shroud of the forward curved fan without shroud, the rotating stall cells formed due to the blade tip leakage vortex. The cell rotated with 40% rotation speed of the impeller, and formed the pseudo seven blades in the circumferential direction of the impeller.
2. The fan having impeller with shroud (MF9S) hardly forms the rotating stall cells. The uniform aerodynamic noise source was formed around the front shroud of the impeller. From these results, the broadband noise level of MF9S in the low frequency domain became large than that of the MF9 at the vicinity of the rotating frequency of the rotating stall cell.
3. The outward flow hardly formed due to the leakage vortex at the blade tip side of MF9, so that the main flow domain reduced. The static pressure of MF9 with rotating stall cell induces the pressure drop due to the decrease of the main flow domain.
4. The relation between the aerodynamic characteristics and noise became the trade-off, however, we clarified experimentally that the comprehensive characteristics of the MF9S are improved in the high flow rate domain.

REFERENCE

[1] http://www.mlit.go.jp/en/index.html (accessed on 1. Nov. 2014)

[2] Q. Datong, M. Yijun, L. Xiaoliang, Y. Minjian － *Experimental study on the noise reduction of an industrial forward - curved blades centrifugal fan***,** Applied Acoustics, **2009**

[3] Velarde-Suárez, S., Santolaria-Morros, C., and Ballesteros-Tajadura, R. － *Experimental Study on the Aeroacoustic Behavior of a Forward-Curved Blades Centrifugal Fan,* ASME Journal of Fluids Engineering, Vol. 121, No. 2, **1999**

[4] Velarde-Suárez, S., Ballesteros-Tajadura, R., Hurtado-Cruz, J. P., and Santolaria-Morros, C. － *Experimental determination of the tonal noise sources in a centrifugal fan*, Journal of Sound and Vibration, Vol. 295, **2006**

[5] Velarde-Suárez, S., Ballesteros-Tajadura, R., Santolaria-Morros, C., and Pereiras-García, B. － *Reduction of the aerodynamic tonal noise of a forward-curved centrifugal fan by modification of the volute tongue geometry*, Applied Acoustics, Vol. 69, No. 3, **2008**

[6] Y. Ohta, E. Outa amd K. Tajima - E*valuation and Prediction of Blade-Passing Frequency Noise Generated by a Centrifugal Blower*, Journal of Turbo Machinery, Vol. 118, No. 3, **1996**

[7] M. Younsi, F. Bakir, S. Kouidri, and R. Rey － *Influence of Impeller Geometry on the Unsteady Flow in a Centrifugal Fan: Numerical and Experimental Analyses*, International Journal of Rotating Machinery, Vol. 2007, **2007**

[8] R. E. Longhouse – *Control of tip-vortex of axial flow fans by rotating shrouds,* Journal of Sound and Vibration, Vol.58, No. 2, **1978**

[9] J. E. Ffowcs Williams and D. L. Hawkings － *Sound generation by turbulence and surfaces in arbitrary motion*, Philosophical Transactions of the Royal Society of London. Series A, vol. 264, No. 1151, **1969**

[10] A. Powell － *Theory of Vortex Sound*, Journal of the Acoustic Society of America, Vol. 36, No. 1, **1964**

[11] M. S. Howe － *Theory of Vortex Sound*, Cambridge University Press, Cambridge, **2003**

NOMENCLATURES

b; span length (mm)

BPF; Blade Passing Frequency

C; chord (mm)

c; speed of sound (m/s)

CAD; Computer Aided Design

CFD; Computational Fluid Dynamics

D; diameter of impeller (mm)

EFD; Experimental Fluid Dynamics

f; frequency (Hz)

FFT; Fast Fourier Transform

L; shaft power (W)

L_p; sound pressure level (dB)

The sound pressure level is defined as the following;

$$L_p = 10\log\left(\frac{p^2}{p_0^{\,2}}\right)$$

where, p (Pa) is the sound pressure, p_0 is the lowest sound pressure (20 μPa).

L_A; noise level (dB (A))

The noise level is defined as the sound pressure level corrected by the A-weighted curve (see IEC 61672).

L_{SA}; specific noise level (dB)

The specific noise level can estimate the total performance of the fan; this level is defined as the following equation.

$$L_{SA} = L_A + 10\log\left(Q\,P_t^{\,2}\right) + 20$$

where, Q (m^3/min) is the flow rate, P_t (Pa) is the total pressure of the fan.

LES; Large Eddy Simulation

N; rotation speed (rpm)

N_c; rotation speed of rotating cell

P_s; static pressure (Pa)

p_a; sound pressure (Pa)

Q; flow rate (m^3/min）

U; circumferential velocity (m/s)

Z; number of blades

Z_c; number of rotation cell

z; axial direction distance (mm)

$\vec{u}$; velocity vector （m/s）

$\vec{\omega}$; vorticity vector （1/s）

φ; flow rate coefficient

ψ_s; static pressure coefficient

λ; power coefficient

η; efficiency

ρ; density of air (kg/m^3)